HHS Public Access

Author manuscript

J Am Chem Soc. Author manuscript; available in PMC 2015 August 13.

Published in final edited form as:

J Am Chem Soc. 2009 March 11; 131(9): 3260–3270. doi:10.1021/ja807969a.

Substrate–Protein Interaction in Human Tryptophan Dioxygenase: The Critical Role of H76

Dipanwita Batabyal and **Syun-Ru Yeh**

Department of Physiology and Biophysics, Albert Einstein College of Medicine, 1300 Morris Park Avenue, Bronx, New York 10461

Syun-Ru Yeh: syeh@aecom.yu.edu

Abstract

The initial and rate-limiting step of the kynurenine pathway in humans involves the oxidation of tryptophan to *N*-formyl kynurenine catalyzed by two hemeproteins, tryptophan 2,3-dioxygenase (hTDO) and indoleamine 2,3-dioxygenase (hIDO). In hTDO, the conserved H76 residue is believed to act as an active site base to deprotonate the indole NH group of Trp, the initial step of the Trp oxidation reaction. In hIDO, this histidine is replaced by a serine. To investigate the role of the H76, we have studied the H76S and H76A mutants of hTDO. Activity assays show that the mutations cause a decrease in k_{cat} and an increase in K_M for both mutants. The decrease in the k_{cat} is accounted for by the replacement of the active site base catalyst, H76, with a weaker base, possibly a water, whereas the increase in K_M is attributed to the loss of the specific interactions between the H76 and the substrate as well as the protein matrix. Resonance Raman studies with various Trp analogs indicate that the substrate is positioned in the active site by the ammonium, carboxylate, and indole groups, via intricate H-bonding and hydrophobic interactions. This scenario is consistent with the observation that L-Trp binding significantly perturbs the electronic properties of the O_2-adduct of hTDO. The important structural and functional roles of H76 in hTDO is underscored by the observation that the electronic configuration of the active ternary complex, L-Trp-O_2-hTDO, is sensitive to the H76 mutations.

Introduction

Tryptophan 2,3-dioxygenase (TDO) is a heme-containing enzyme that catalyzes the oxidative cleavage of tryptophan (Trp) to *N*-formyl kynurenine (NFK), the initial and rate-limiting step of the kynurenine pathway, by adding both oxygen atoms of dioxygen to the C_2=C_3 bond of the indole moiety of Trp as illustrated in Scheme 1.[1–6] Trp is the scarcest essential amino acid in mammals. The majority of our dietary Trp (~95%) is metabolized along the kynurenine pathway in the liver by TDO, which ultimately leads to the biosynthesis of NAD and NADP.[7] A small amount of the Trp (~1%) is used to synthesize the neurotransmitter serotonin.[8] Consequently, TDO plays a critical role in determining the relative Trp flux in the serotonergic and kynurenic pathways.

Correspondence to: Syun-Ru Yeh, syeh@aecom.yu.edu.

Supporting Information Available: Complete ref 21 and supporting figures. This material is available free of charge via the Internet at http://pubs.acs.org.

Indoleamine 2,3-dioxygenase (IDO) is another heme-containing enzyme that catalyzes the same reaction of Trp.[9] It is primarily present in mammals and is ubiquitously distributed in all tissues other than liver.[2,9,10] In contrast, TDO is mainly present in liver and has not only been found in mammals but also in mosquitoes and bacteria.[1–3,11,12] The expression of IDO is induced by interferon-γ (IFN-γ) and is closely linked to a wide spectrum of immune-related pathophysiological conditions,[1,8,10,13] whereas TDO is inducible by glucocorticoid hormones and is regulated by the availability of the physiological substrate, Trp.[14,15] Despite the fact that IDO and TDO catalyze the same reaction, they share very low sequence homology (~10%), and exhibit distinct biochemical properties. IDO oxidizes L-Trp, D-Trp, and various indoleamine derivatives, whereas TDO is more specific for L-Trp.[1,2,16,17] IDO can bind oxygen, independent of the presence or absence of the substrate, whereas TDO only forms stable oxygen complex in the presence of Trp.[1,18,19]

Although IDO and TDO were discovered several decades ago, their crystallographic structures were not resolved until recently.[20–22] The structure of the human isoform of IDO (hIDO) is monomeric, with two α-helical domains sandwiching the prosthetic heme group.[20] The proximal heme binding pocket is primarily made up of four long α-helices from the larger domain, in which the heme iron is coordinated by an evolutionary conserved histidine residue, H346. On the other hand, the structures of two bacterial isoforms of TDO (xcTDO and rmTDO from *Xanthomonas campestris* and *Ralstonia metallidurans*, respectively),[20–22] which are believed to be structurally analogous to that of the human isoform (hTDO), are tetrameric, with one heme per monomer. As the L-Trp-bound structure is only available for xcTDO, hereafter, the structure-related discussions will be based on the structure of xcTDO.

In xcTDO, the heme is coordinated by H240, an absolutely conserved residue in TDO. [21,23] Despite the low sequence homology between xcTDO and hIDO, xcTDO exhibits high structural similarity with the large domain of hIDO. Structure-based sequence alignment shows that most of the critical residues involved in substrate–protein interactions in xcTDO and hTDO are conserved in hIDO.[21,22] Nonetheless, the evolutionarily conserved H55 in xcTDO, which has been implicated in the initial deprotonation of the indole NH group of the substrate during the oxygen reaction,[24] is replaced by a serine in hIDO. As this serine residue is also absolutely conserved in the IDO family of enzymes, the oxygen reaction carried out by hIDO is believed to proceed via a mechanism distinct from that of hTDO.[24] Comparative studies of hIDO and hTDO carried out by Batabyal and Yeh suggest that the active base critical for the deprotonation of the substrate in hIDO is the heme-bound O_2, in contrast to the H76 in hTDO (corresponding to the H55 in xcTDO), as illustrated in the cartoon shown at the bottom of Scheme 1.[24,25]

Recently, hIDO has been recognized as an important drug target for cancer and neurological disorders;[8,10,13,26–28] it is hence important to understand the structural and functional properties of hIDO as compared to hTDO to develop a potent inhibitor specifically targeting hIDO. In this work, we sought to evaluate the structural and functional role of the H76 in hTDO by systematically investigating the H76S mutant, a mimic of hIDO, and the H76A mutant. For the structural studies, a diatomic heme ligand, CO, along with various substrate analogs were used as active site probes. Resonance Raman and optical absorption

spectroscopies were employed to monitor the substrate–protein interactions in the mutants as compared to the wild type protein. The functional properties were assessed by steady-state activity measurements, along with Michaelis–Menten analysis. The active ternary complex, L-Trp-O_2-hTDO, was identified for the first time and shown to be sensitive to the mutation in the H76 residue. The data are integrated and discussed in the context of the enzymatic mechanism of this fascinating dioxygenase.

Materials and Methods

All chemicals, other than Trp, used for this study were of analytical reagent grade from Sigma-Aldrich Corp. (St. Louis, MO) unless otherwise indicated. L- and D-Trp were obtained from Fluka Chemical Corp. (Ronkonkama, NY). O_2, CO, and Ar were obtained from Tech Air (White Plains, NY). The $^{13}C^{18}O$ isotope was purchased from Icon Isotopes (Summit, NJ). All the chemicals were used without further purification, and prepared with deionized water (Millipore).

Cloning, Expression, and Purification of the Wild Type hTDO

Full-length hTDO has a high tendency to aggregate in free solution and to form inclusion bodies when expressed in *Escherichia coli*. To overcome these problems, we have designed a truncated version of hTDO by using the sequences of xcTDO and paTDO (from *Pseudomonas aeruginosa*) as a guide. In this new construct the 1–17 and 389–406 fragments were deleted, as they are not present in the bacterial TDOs (Figure S1, Supporting Information), indicating that they might not be critical for the structure and function of hTDO. Indeed, with this new construct, we were able to produce a soluble, yet fully functional form of hTDO.[24]

The cDNA of hTDO, with N- and C-termini truncated and a hexa-histidine tag attached to the C-terminus, was cloned into a pET14b vector and transformed into *E. coli* BL21(DE3). The transformant was selected from a single colony on a LB kanamycin agar plate and was used to inoculate a LB medium, supplemented with 50 μg/mL kanamycin. This starter culture was grown overnight at 37 °C, and was subsequently used to inoculate a 1 L LB medium. The resulting *E. coli* culture was grown at 37 °C in a shaker at 250 rpm until the optical density at 600 nm reached ~0.8. The expression of hTDO was induced by isopropyl 1-thio β galacto-pyranoside (IPTG), with a final concentration of 1 mM. An aliquot of hemin, with a final concentration of 8–10 μM, was added to the culture to ensure the complete incorporation of the heme prosthetic group into the recombinant protein. The culture was grown at 25 °C for additional 6–8 h in a shaker at 150 rpm. The cells were harvested by centrifugation and stored at −20 °C until use.

The cell pellet thus prepared was resuspended in pH 7.8 lysis buffer (300 mM NaCl, 50 mM K_2HPO_4, 10 mM L-Trp, and 5% glycerol), supplemented with protease inhibitors (Roche). The suspension was sonicated in an ice bath, following incubation with lysozyme and DNaseI (10 and 0.2 mg per liter culture, respectively) for 30 min at 4 °C. The cell lysate was centrifuged twice at 18 000 rpm for 30 min. The supernatant was collected and loaded onto a Ni-NTA column (Novagen). The column was washed with ~15 column-volumes of lysis buffer, followed by a sequential wash with 10, 30, and 60 mM imidazole in lysis buffer (5

column-volumes each). The protein was eluted with 250 mM imidazole in lysis buffer. The imidazole was subsequently removed by overnight dialysis. The purified protein was frozen in aliquots and stored in liquid nitrogen until use.

To stabilize the protein and minimize aggregation, 10 mM L-Trp and 5% glycerol were present throughout the whole course of the purification process. Before each experiment, L-Trp and glycerol were removed by passing the protein through a G25 column, followed by a sequential wash with a 10K Centricon (Millipore). The complete removal of the L-Trp was confirmed by resonance Raman spectroscopy, which is sensitive to the presence of L-Trp. The protein was purified to near homogeneity as indicated by the SDS-PAGE (12%) data and the elution profile from a size-exclusion column (Supedex 200) attached to an AKTA Purifier (Amersham Biosciences) (see Figure S2 in the Supporting Information), with a yield of ~12 mg per liter of *E. coli* culture.

Shortly after our initial report on the wild type truncated hTDO,[24] Basran et al. reported the expression, purification, and functional studies of the full-length hTDO.[29,30] They showed that the protein can be expressed in a mixture of apo and holo form; in addition, its activity can be introduced by reconstituting it with hemin. The k_{cat} and K_M values of the reconstituted protein toward L-Trp were reported to be similar to the values we obtained from the truncated version of hTDO,[24,29] despite the fact that for their assay a mixture of methylene and ascorbate was used as the reductant[29] (instead of a typical protocol with ascorbate alone used by us[24] and others[5,18,22,30–34]). Intriguingly, the activity of the full-length enzyme toward D-Trp, reported by Basran et al., is extremely low and is only detectable with a saturating concentration of D-Trp (50 mM). In contrast, with our enzyme, we were able to observe significant activity with a wide range of D-Trp concentrations.[24] To account for the disparity, Basran et al. argued that the higher affinity and activity toward D-Trp observed in our assay is a result of residual L-Trp remaining in our enzyme solution, as L-Trp was used throughout our purification procedure. Although this is a legitimate concern, it can be fully ruled out; to avoid the possible contamination by L-Trp, prior to each experiment we treated the sample with a thorough cleaning procedure, and the complete removal of the L-Trp was confirmed by resonance Raman spectroscopy, as described above. More importantly, consistent with our observations, other mammalian TDO has been shown to be reasonably active toward D-Trp.[33] In addition to its much lower activity toward D-Trp, the full-length hTDO prepared by Basran et al. showed two distinct features as compared to our enzyme: (1) the ferrous deoxy protein exhibited a six-coordinate low-spin configuration, in contrast to a more typical five-coordinate high-spin heme of our enzyme;[24] and (2) the O_2-complex is not observable upon mixing the deoxy enzyme with O_2, in contrast to the meta-stable nature of our O_2-adducts (*vide infra*). While the origin of the unique results from Basran et al. remains to be investigated, it is important to note that N-terminal truncation in rat liver TDO, which is not stable in its full-length form,[30,35] did not affect its spectroscopic properties as well as its activity.[30] Likewise, N-terminal truncation in rmTDO was shown to improve its solubility and stability, without affecting the integrity of its overall structural properties.[22] These data fully support the reliability of our enzyme preparation.

Expression and Purification of the H76S and H76A Mutants of hTDO

The H76S and H76A mutations were created by using the QuikChange II kit (Stratagene). The sequences were verified by DNA sequence analysis. The mutants were cloned, expressed, and purified by using the same protocol as that described for the wild type protein.

Steady-State Activity Assay

For the activity assay, the ferric hTDO was rapidly mixed with sodium ascorbate (100-fold excess with respect to the protein) in the presence of a desired amount of L-Trp in pH 7.0 phosphate buffer (100 mM) at room temperature. The final concentration of hTDO was 3.5 μM for H55S and 0.5 μM for H55A. The reaction rate was followed by monitoring the product formation at 321 nm (ε = 3750 $M^{-1}cm^{-1}$ for *N*-formyl kynurenine).[18,24] The initial product formation rate was plotted as a function of L-Trp concentration; the data were analyzed by Michealis-Menten curve fitting with Origin 6.1 software (Microcal Software, Inc., MA).

Spectroscopic Measurements

The optical absorption spectra were taken on a spectrophotometer, UV2100, from Shimadzu Scientific Instruments, Inc. (Columbia, MD) with a spectral slit width of 1 nm. The resonance Raman spectra were taken on the instrument described elsewhere.[36] Briefly, the 413.1 nm excitation from a Kr ion laser (Spectra Physics, Mountain View, CA) was focused to a ~30 μm spot on the spinning quartz cell rotating at ~1000 rpm. The scattered light, collected at a right angle to the incident laser beam, was focused on the 100 μm-wide entrance slit of a 1.25 m Spex spectrometer equipped with a 1200 grooves/mm grating (Horiba Jobin Yvon, Edison, NJ), where it was dispersed and then detected by a liquid nitrogen-cooled CCD detector (Princeton Instruments, Trenton, NJ). A holographic notch filter (Kaiser, Ann Arbor, MI) was used to remove the laser line. The Raman shift was calibrated by using indene (Sigma) as a reference. The laser power was kept at ~5 mW for all measurements, except that used for the CO complexes, in which it was kept at ~1–2 mW to avoid photodissociation of the heme-bound CO. The acquisition time was ~20–30 min for all the spectra obtained.

The ferrous derivative was prepared by reducing the ferric protein, prepurged with Ar gas, with sodium dithionite under anaerobic conditions. The CO-bound ferrous complexes were obtained by injecting CO gas into the reduced enzyme with a gastight syringe. The concentration of the protein samples used for the Raman measurements was ~15–50 μM in pH 7.0 phosphate buffer (100 mM).

Stopped-Flow Measurements

The kinetic measurements were performed at 25 °C with a π*180 stopped-flow instrument, equipped with a photodiode array detector, from Applied Photophysics Inc. (Leatherhead, UK). To ensure the absolute anaerobic conditions, prior to each experiment, the entire solution flow-path in the stopped-flow system was flushed with an anaerobic sodium dithionite solution several times with gastight syringes. At the last run, the anaerobic sodium

dithionite solution was allowed to sit for 30 min to quench any residual oxygen. The dithionite solution was subsequently washed away with Ar-purged anaerobic buffer, prior to sample loading. The ferrous deoxy derivative of hIDO was prepared by reducing the ferric enzyme, prepurged with argon gas, with a stoichiometric amount of sodium dithionite in an anaerobic buffer, as guided by optical absorption measurements. All the deoxy samples were transferred with gastight syringes to the stopped-flow system. For the L-Trp-bound enzyme, hTDO was incubated with desired amount of L-Trp at least for 2 h prior to each measurement. All experiments were performed in pH 7.0, phosphate buffer (100 mM). The stopped-flow data were analyzed by using ProK software from Applied Photophysics Inc. (Leatherhead, UK).

Results and Discussion

Structural Properties of the H76S and H76A Mutants

As shown in Figure 1A, the ferric derivative of H76S has a Soret maximum at 403 nm and a charge-transfer band at 630 nm, typical for a six-coordinate water-bound heme species. The ferrous protein displays a Soret maximum at 431 nm and a visible band at 554 nm, consistent with a five-coordinate high-spin heme. The CO-complex, on the other hand, exhibits a Soret maximum at 418 nm, with α/β bands at 567/535 nm, indicating a six-coordinate low-spin heme. These spectral features are somewhat different from those of the wild type protein as summarized in Table 1, suggesting that the mutation in the H76 residue to serine slightly perturbs the electronic properties of the enzyme. As shown in Figure 1B, the spectral features of the H76A mutant are almost identical to those of the H76S mutant, indicating that the electronic perturbation is not sensitive to the nature of the substituent of the H76 residue.

In the H76S mutant, L-Trp-binding to the ferric derivative causes the Soret to shift from 403 to 408 nm and the charge transfer band at 630 nm to disappear, which are concurrent with the appearance of a broad absorption at ~500–600 nm (Figure 1C). The data indicate a high-spin to low-spin transition, plausibly due to partial deprotonation of the heme-bound water, as that suggested for the wild type protein.[24] L-Trp binding to the ferrous deoxy and CO-derivatives, on the other hand, only causes minute changes to the spectra. These changes induced by L-Trp binding are similar to those observed in the wild type enzyme.[24] In contrast, in the H76A mutant, substrate binding hardly perturbs the spectra of the various derivatives (Figure 1D).

To further evaluate the structural role of the H76 residue, resonance Raman studies were conducted. The general characteristics of the resonance Raman spectra of heme-proteins have been well established.[36–40] In the high frequency region, the spectrum is dominated by the totally symmetric porphyrin in-plane vibrational modes. The ν_2 mode in the 1550 and 1600 cm^{-1} region is sensitive to the spin-state of the heme iron.[36–38] The ν_3 mode in the 1475–1520 cm^{-1} region is sensitive to both the spin-state and the axial-coordination state of the iron. On the other hand, the strong ν_4 mode in the 1350 and 1400 cm^{-1} region is sensitive to the oxidation state of the iron as well as the π-electron density of the porphyrin macrocycle. Additional bands in the low frequency region of the spectrum (200–1000 cm^{-1}), including iron-ligand stretching modes, bending modes associated with the

propionate and vinyl groups peripheral to the heme and heme out-of-plane modes, offer valuable structural information regarding the active site structures of heme-proteins, as these modes are typically sensitive to H-bonding, hydrophobic and/or steric interactions imposed on the heme group by its surrounding protein matrix.

Figure 2 shows the resonance Raman spectra of the ferric H76S and H76A in the presence and absence of L-Trp, as compared to the wild type protein. For all the substrate-free enzymes, the strongest band is ν_4 at 1371 cm^{-1}, indicating a six-coordinate ferric heme. The ν_3/ν_2 bands at 1480/1560 cm^{-1} and 1506/1583 cm^{-1} are characteristic of a six-coordinate high-spin and low-spin heme, respectively.[37,38] The mixed-spin character of the ferric heme indicates that the iron is coordinated with a water molecule in the distal position, consistent that concluded from the optical absorption data. L-Trp binding to the H76A mutant causes a considerable enhancement of the six-coordinate low-spin bands as indicated by the relatively stronger intensities of the low-spin marker lines at 1506/1583 cm^{-1}. The data suggest that L-Trp binds in the vicinity of the heme-bound water, lowers its pK_a and partially converts the weak field ligand, water, to a strong field ligand, a hydroxide. In the H76S mutant, the addition of L-Trp triggers a more pronounced transition to a mostly low-spin species, similar to that reported for hIDO.[25] For hIDO, Terentis et al. proposed that the spin-transition is a result of the deprotonation of the heme-bound water by the indole NH group of the L-Trp.[25] Likewise, we hypothesize that the mutation of the H76 to Ser causes the indole ring of the L-Trp to move closer to the heme-bound water, favoring the hydroxide-bound configuration in hTDO. Consistent with this hypothesis, in hIDO, two $\nu_{Fe\text{-}OH}$ modes were identified at 496 and 546 cm^{-1} in the L-Trp-bound ferric enzyme, but not in the substrate-free enzyme, based on H_2O–D_2O substitution experiments.[25] Comparable isotope substitution experiments were performed with the wild type and the mutants of hTDO; unfortunately, no $\nu_{Fe\text{-}OH}$ modes could be identified, presumably due to their weak Raman cross-sections. An analogous L-Trp binding-induced spin transition has also been reported for TDOs from *Pseudomonas* and rat liver,[41,42] suggesting that it is a general feature for the IDO/TDO-type of enzymes.

In the low frequency region of the wild type spectrum, the 677 and 340 cm^{-1} bands are assigned to the ν_7 and ν_8 modes, respectively, whereas the bands at ~387 and 423 cm^{-1} are attributed to the bending modes of the propionate ($\delta_{propionate}$) and vinyl (δ_{vinyl}) groups of the heme, respectively.[43] The mutation of the H76 to serine or alanine does not significantly affect these modes. L-Trp binding to the wild type hTDO leads to the splitting of the δ_{vinyl} mode to 423 and 431 cm^{-1} and the $\delta_{propionate}$ mode to 376 and 387 cm^{-1}.[24] These spectral changes are consistent with the crystallographic data of the L-Trp-bound xcTDO, in which one of the two propionate groups of the heme forms an H-bond with the ammonium group of the L-Trp. In contrast to the wild type protein, L-Trp binding in either of the two mutants does not bring about noteworthy changes to the low frequency modes, indicating H76 plays an important role in positioning the substrate in the active site of hTDO.

Steady-State Activity of the H76S and H76A Mutants

To examine the activity of the mutants, the oxidized enzymes were rapidly mixed with a desired amount of L-Trp in the presence of 100-fold excess of sodium ascorbate (as a reductant). The product formation was followed as a function of time by monitoring the

absorbance change at 321 nm (ε = 3750 $M^{-1}cm^{-1}$ for NFK).[24] The initial linear rate for the product formation is plotted as a function of L-Trp concentration in Figure 3. The Michaelis–Menten equation fit of the data show that the k_{cat} and K_M values of the H76S mutant are 0.03 s^{-1} and 1.2 mM, respectively, whereas those of the H76A mutant are 0.2 s^{-1} and 0.5 mM, as listed in Table 2. As compared to the wild type enzyme (with k_{cat} and K_M of 2.1 s^{-1} and 0.2 mM), the mutants display much lower k_{cat} and higher K_M, confirming the important structural role of H76 in controlling the oxygen chemistry of L-Trp. The activity of the H76S and H76A mutants toward D-Trp has also been examined; in contrast to L-Trp, neither mutant shows detectable activity toward D-Trp.

Recent crystallographic studies of the H55S and H55A mutants of xcTDO revealed two active site water molecules.[44] The first water molecule was found in the ligand binding site ~3.5A away from the heme iron, similar to that observed in the wild type protein.[21] This water molecule, like that in the wild type protein (see Figure 4), forms H-bonds with the ammonium and indole NH groups of the L-Trp, as well as the backbone NH group of the G125. The second water molecule occupies the space vacated by the H55 side chain. In the H55A mutant, this water forms an H-bond with the indole NH group, whereas that in the H55S mutant, is situated further away from the indole NH group and forms an H-bond with the S55. We hypothesize that a water molecule, comparable to the second water in xcTDO, is present in the H76S and H76A mutants of hTDO and acts as a base to deprotonate the indole group of the substrate, accounting for the residual activities of the mutants. We attribute the much lower k_{cat} value of the H55S mutant to a longer distance between the water and the heme-bound ligand as implicated by the crystallographic data of the H55S and H55A mutants of xcTDO.[44]

The function of an active site water as a base catalyst is not unprecedented. In a nonheme dioxygenase, MhpB, from *E. coli*, an active site residue, H115, is believed to act as acid/base catalyst during the enzymatic reaction. The residual activity found in the H115A mutant of MhpB has been attributed to an alternative catalysis by a solvent water molecule bound in the site normally occupied by H115.[45] Likewise, the role of solvent water molecules in enzyme catalysis has been widely recognized in the reactions of heme containing oxygenases, such as P450, nitric oxide synthase, and heme oxygenase.[46–49]

Although the active species for the dioxygenase reaction of hTDO is the ferrous enzyme, Batabyal and Yeh reported that the ferric wild type hTDO exhibits significant activity toward L-Trp, but not D-Trp.[24] Although the origin of the activity remains unclear, similar activity of the ferric hTDO toward L-Trp was later reported by Basran et al.[29] In contrast, for the H76S and H76A mutants, the ferric derivatives shows no activity toward either L-Trp or D-Trp, further highlighting the critical role of the H76 residue in hTDO.

Ternary Complex of hTDO

To gain a better understanding of the oxygen chemistry of hTDO, the active ternary complex (L-Trp-O_2-hTDO) of the wild type and the H76S and H76A mutants were examined with a stopped-flow system, equipped with a photodiode detector. For this set of the experiments, the ferric enzyme was first purged with argon and titrated with a stoichiometric amount of dithionite. The complete reduction of the sample was confirmed by *in situ* absorption

measurements. The reduced deoxy derivative of the enzyme was transferred to the stopped-flow instrument, maintained under anaerobic conditions, where it was mixed with the aerobic phosphate buffer (pH 7.0). The progression of the reaction was monitored by optical absorption measurements. As a control experiment, the deoxy enzyme was mixed with an argon-saturated buffer. The optical absorption spectrum obtained following the mixing exhibits the typical Soret and visible bands for the pure deoxy species (data not shown), which remained stable within the time window monitored (~100 s), confirming the anaerobicity and the reliability of the stopped-flow measurements.

As a first step, the O_2-complex of the substrate-free wild type enzyme was examined. As shown in Figure 5A, in the absence of L-Trp, the wild type ferrous enzyme spontaneously autooxidizes to the ferric derivative upon exposure to oxygen. The lack of clear isosbestic points suggests that the autoxidation reaction goes through an intermediate state. To resolve the intermediate, the time-resolved data were fitted with a three-state sequential model by using a global-fitting software, ProK (Applied Photophysics Inc.). The residuals from the fitting are negligible, confirming the reliability of the model.

Figure 5B shows the best fitted standard spectra of the three species. They display Soret maxima at 431, 412, and 407 nm, respectively, which are assigned to the deoxy ferrous, O_2-complex and ferric species, respectively. Intriguingly, the β/α bands in the 500–600 nm region, typical for a six-coordinate low-spin O_2-bound ferrous heme, are too weak to be observed. Nonetheless, the data indicate that the deoxy protein binds O_2 to form the O_2-complex, which subsequently autooxidizes to the ferric species by releasing the dioxygen as superoxide. The best fitted rate constants associated with the two reactions are 1.38 and 0.13 s^{-1}. The much slower autoxidation rate as compared to the O_2-binding rate leads to a maximum of ~80% population of the O_2-complex transiently, as may be seen in the insert of Figure 5B.

In the presence of L-Trp, the O_2-complex of hTDO is much more stable, perhaps due to the fact that, in the presence the substrate, the active site is completely devoid of solvent molecules, which retards the autoxidation process. As shown in Figure 6, the Soret maximum of the O_2-adduct is located at 417 nm in the presence of L-Trp, which is 5 nm higher than its absence; in addition, the two visible bands, β/α, are now fully visible at 543/576 nm. The unique spectral feature introduced by L-Trp binding indicates that the L-Trp bound in the active site is important in modulating the electronic properties of the O_2-heme moiety. The spectroscopic properties of the ternary complex of hTDO are similar to those reported for a bacterial TDO analog (pfTDO) from *Pseudomonas fluorescens*, which exhibited a Soret maximum at 418 nm and visible bands at 545 and 580 nm.[18,50] Although, unlike hTDO, in the absence of the substrate the O_2-compex of pfTDO auto-oxidized to the ferric form without populating a transient oxygen intermediate.

The active ternary complexes of the H76S and H76A mutants of hTDO, like the wild type protein, are stable enough to be detected spectroscopically. As shown in Figure 6, the H76S mutant exhibits a Soret maximum of 417 nm, similar to that of the wild type protein. However, its bandwidth is significantly broader and the intensity of the α band is notably reduced with respect to that of the β-band. On the other hand, in the H76A mutant, the Soret

maximum and α band shift to 416 and 572 nm, respectively, with respect to the wild type enzyme, while the β band remains at almost the same position, but with a relatively lower intensity. The sensitivity of the spectral features of the active ternary complex of hTDO to the mutations of the H76 residue is consistent with the proposed structure of the active ternary complex[24] shown in the right panel of Figure 6. Taken together, the data demonstrate that the modulation of the electronic properties of the O_2-heme moiety introduced by L-Trp is mediated via the H76 residue.

Substrate–Protein Interactions

To understand, from a structural point of view, how the substrate–protein interactions influence the electronic properties of the O_2-heme moiety in the active ternary complex of hTDO, and how the interactions are regulated by the H76 residue, we employed CO as a structural probe for the active site of the enzyme.

CO has been recognized as an excellent structural probe for the distal ligand binding pocket of hemeproteins, as the Fe–CO and C–O bond strengths are modulated by interactions between the heme-bound CO and its immediate surroundings. In general, the Fe–C–O moiety can be represented by two extreme structures.

$$\mathrm{Fe}^{\delta-}-\mathrm{C}\equiv\mathrm{O}^{\delta+}(\mathrm{I})\leftrightarrow\mathrm{Fe}{=}\mathrm{C}{=}\mathrm{O}(\mathrm{II}) \quad (1)$$

When CO is exposed to positive polar surroundings, instead of a hydrophobic or negative polar environment, the form (I) is destabilized.[51] As a result the bond-order of the Fe-CO bond is higher, which is concurrent with a lower C–O bond order. On this basis, the $\nu_{\mathrm{Fe\text{-}CO}}$ and $\nu_{\mathrm{C–O}}$ frequencies are inversely correlated, which can be used as a quantitative measure of the electrostatic potential of the ligand binding site of hemeproteins.[36,38,51–54]

With resonance Raman spectroscopy, Batabyal and Yeh showed that in the wild type substrate-free hTDO, the $\nu_{\mathrm{Fe\text{-}CO}}$ and $\nu_{\mathrm{C–O}}$ are at 496 and 1958 cm^{-1}, respectively.[24] L-Trp binding causes them to shift to 488 and 1972 cm^{-1}, indicating a low electrostatic potential surrounding the CO. In contrast, in hIDO, the $\nu_{\mathrm{Fe\text{-}CO}}$ and $\nu_{\mathrm{C–O}}$ are at 518 and 1933 cm^{-1}, respectively; upon L-Trp binding, they shift to 542 and 1901 cm^{-1}, indicating a positive polar electrostatic potential surrounding the CO.[25] On the basis of these data, it was proposed that in hIDO the indole NH group of the L-Trp forms an H-bond with the CO,[25] whereas in hTDO the NH group of the L-Trp donates an H-bond to the H76 side chain, forcing the aromatic ring of the indole side chain to face the CO.[24] Extending from that work, in the current study we systematically investigated the substrate–protein interactions in hTDO by using CO along with Trp and Trp analogs, including L-Trp, D-Trp, tryptamine (TAM), and indole propionic acid (IPA), as structural probes. The structures of the Trp analogs employed are shown in Scheme 2. The role of the H76 residue in regulating the substrate–protein interactions are evaluated by examining the H76S and H76A mutants with respect to the wild type protein.

Figure 7 shows the low frequency Raman spectra of the CO-complexes of the wild type and the H76S and H76A mutants of hTDO, in the presence or absence of Trp or Trp analogs.

The assignments of all the $\nu_{Fe\text{-}CO}$ modes were confirmed by $^{12}C^{16}O$–$^{13}C^{18}O$ isotope substitution experiments (see Figure S3A in the Supporting Information). To interpret the Raman data in a quantitative fashion, the $\nu_{Fe\text{-}CO}$ modes were deconvoluted into a minimum set of Gaussian peaks, as shown in Figure 8.

In the substrate-free wild type protein, the broad $\nu_{Fe\text{-}CO}$ mode at ~496 cm^{-1} can be deconvoluted into three peaks at 485, 500, and 517 cm^{-1} (Figure 8, panel A1), whereas those of the H76S and H76A mutants are made up by two peaks at 491/517 and 490/515 cm^{-1}, respectively (Figure 8, panel B1 and C1). The small peak at 514 cm^{-1} (shaded in gray), which is present in all the spectra, is assigned to an intrinsic heme mode, as it does not shift upon $^{12}C^{16}O$–$^{13}C^{18}O$ isotope substitution.[24]

The binding of Trp (or Trp analogs) to the wild type protein and mutants introduces distinct spectral changes to the $\nu_{Fe\text{-}CO}$ modes, which are sensitive to the structure of the Trp/Trp analogs employed. On the basis of the L-Trp-bound xcTDO structure shown in Figure 4, the binding of Trp or Trp analogs may lead to four possible Fe-CO conformers, as summarized in the left scheme, in which the Fe-ligand moiety faces (i) the aromatic indole ring of the L-Trp, (ii) the NH group of the G152 residue (corresponding to G125 in the xcTDO structure shown in Figure 4), (iii) the ammonium group of the L-Trp, and/or (iv) the indole NH-H76 pair.

In the wild type protein, L-Trp binding causes the merging of the three $\nu_{Fe\text{-}CO}$ components into one sharp peak at 488 cm^{-1}, along with the appearance of a small peak at 502 cm^{-1} (Figure 8, panel A5). They are assigned to the conformer-i and conformer-iv, respectively. The linewidths of both peaks are significantly reduced as compared to those found in the substrate-free enzyme, indicating reduced conformational freedom of the Fe–C–O moiety due to the restriction imposed by the L-Trp. The binding of D-Trp (Figure 8, panel A4), on the other hand, leads to the merging of the three $\nu_{Fe\text{-}CO}$ components into one main peak at 491 cm^{-1}, assigned to the conformer-i, similar to that induced by L-Trp binding. Nonetheless, as compared to the L-Trp-bound enzyme, the peak position is up-shifted (from 488 to 491 cm^{-1}) and the peak width is increased (from 15 to 20 cm^{-1}); in addition, the minor component at 502 cm^{-1} (conformer-iv) is completely lost. The data suggest that D-Trp is anchored in the distal site in a fashion similar to that of L-Trp, that is, with the aromatic indole ring facing the heme-bound ligand, but the substrate–protein interactions are perturbed due to the change in the stereo-orientation of the side chain group of the substrate.

The binding of IPA, in which the ammonium group of L-Trp is replaced by a hydrogen atom, leads to two peaks at 486 and 515 cm^{-1} (Figure 8, panel A3), assigned to the conformer-i and conformer-ii, respectively. On the other hand, the binding of TAM, in which the carboxylate group is replaced by a hydrogen atom, leads to three peaks at 485, 510, and 525 cm^{-1} (Figure 8, panel A2), assigned to the conformer-i, conformer-ii, and conformer-iii, respectively. It is conceivable that, in the TAM-bound state, the loss of the H-bonding interaction between the carboxylate group and the protein matrix loosens the binary complex, thereby allowing the ammonium group to interact with the heme-bound ligand. The distinct spectral features introduced by IPA and TAM, as compared to L-Trp,

demonstrate the importance of the ammonium and carboxylate group in controlling the substrate–protein interactions in hTDO.

In the H76S mutant, L-Trp binding causes a small shift of the two peaks to 490/514 cm^{-1} (Figure 8, panel B5), as well as the intensity enhancement of the 490 cm^{-1} peak and the broadening of the 514 cm^{-1} peak. The 490 cm^{-1} component, like the 488 cm^{-1} peak in the L-Trp-bound wild type enzyme, is assigned to the conformer-i. Its 2 cm^{-1} higher peak position and considerably broader line width as compared to that of the 488 cm^{-1} peak in the wild type protein (22 vs 15 cm^{-1}) suggest that the tight substrate–protein interactions illustrated in Figure 4 are partially relaxed due to the loss of the H-bond between the H76 and the indole NH group. The 517 cm^{-1} component is assigned to the conformer-ii. In the H76A mutant (Figure 8, panel C5), L-Trp binding leads to a spectrum similar to that of the L-Trp-bound H76S, indicating that the two substrate-bound mutants exhibit similar structures. Consistent with this observation, the $\nu_{C–O}$ modes of the L-Trp-bound H76A and H76S mutants were identified at the same frequency, 1968 cm^{-1}, which is 4 cm^{-1} lower than that of the wild type protein (see Figure S3B in the Supporting Information).

The binding of D-Trp to the H76S and H76 A mutants (Figure 8, Panels B4 and C4) causes the shifts of the two peaks to 492/521 and 493/523 cm^{-1}, respectively, which are assigned to the conformer-i/conformer-iii. The presence of conformer-iii, instead of the conformer-ii observed in the L-Trp-bound protein, indicate that D-Trp is bound in a unique geometry such that its ammonium group may interact with the heme-bound CO. The differences observed in the D-Trp- versus L-Trp-bound states in the mutants are much more significant as compared to that observed in the wild type enzyme, indicating that the substrate stereospecificity is more pronounced in the mutants. The binding of TAM or IPA (Panels B2–3 and C2–3), on the other hand, induces only minute changes to the $\nu_{Fe\text{-}CO}$ mode, as compared to the substrate-free form. They suggest a weak substrate–protein interaction, due to the loss of the H76, as well as the ammonium or carboxolate group of the substrate, the three critical structural components in modulating the substrate–protein interaction in hTDO.

In addition to the obvious perturbations to the $\nu_{Fe\text{-}CO}$ modes as discussed above, the data shown in Figure 7 show that substrate-binding to the wild type and mutants of hTDO introduces spectral shifts and intensity changes to a number of low frequency modes, in particular the $\delta_{propionate}$, δ_{vinyl} and ν_8 at ~389, 428, and 357 cm^{-1}, respectively, as well as the out-of-plane modes at 718/424 cm^{-1}.[58] These spectral changes are sensitive to the structure of the substrate and the mutation in the H76 residue, demonstrating that the structural properties of the heme are closely coupled to the substrate through the H76 residue.

The Raman data reported here are consistent with the crystallographic data of xcTDO. The crystallographic structures of xcTDO show that L-Trp binding introduces significant structural changes to the protein matrix,[21] accounting for the spectral differences between the substrate-free and L-Trp-bound enzyme. In the substrate-bound xcTDO, as shown in Figure 4, the L-Trp is positioned above the distal ligand-binding site by extensive hydrophilic as well as hydrophobic interactions, including: (1) the H-bond between the indole NH group of the L-Trp and the side chain of H55, (2) the H-bonds between the

ammonium and carboxylate groups of the L-Trp and the Y113, R117, and T254, as well as a distal water and a propionate group of the heme, and (3) the hydrophobic interactions between the aromatic indole ring and the hydrophobic clusters involving the L120 and F51, as well as the Y24, Y27, and L28 from a second subunit of the tetrameric enzyme. In addition to forming an H-bond with the indole NH group, the H76 may play a role in maintaining the integrity of the hydrophobic pocket, as its aromatic ring fits perfectly in the back of the hydrophobic pocket housing the indole ring of the substrate (Figure 4). The Raman data demonstrate that the tight interaction between the substrate and the protein is relaxed due to the loss of the H-bond between the H76 and the indole NH group of the L-Trp, as well as the perturbed interaction between the indole ring and the hydrophobic pocket, in the H76S and H76A mutants, and/or the elimination of the ammonium/carboxolate group of the substrate.

Implications in the Oxygen Chemistry of hTDO

In contrast to the monooxygnase reaction of the P450 type of enzymes, the dioxygenase reaction of TDO and IDO are poorly understood despite their physiological importance. Based on the ionic mechanism proposed by Hamilton,[1,55] the first step of the dioxygenase reaction involves the deprotonation of the indole NH group of Trp by an active base (see Figure S4 in the Supporting Information). It is followed by the electrophilic addition of the heme-bound O_2 to the C_2=C_3 bond of Trp, leading to the formation of the heme iron-bound 3-indolenylperoxy intermediate. The peroxy intermediate subsequently converts to the product, NFK, via either the dioxetane intermediate or Criegee type rearrangement.[1,34,55] An alternative radical mechanism, involving electron transfer from the deprotonated L-Trp to the heme-bound O_2, followed by radical recombination to generate the 3-indolenylperoxy intermediate, has also been proposed by Leeds et al.[34] Nevertheless, none of the postulated intermediates, except for the dioxygen-bound intermediate, have been identified experimentally in either IDO or TDO.

The oxygen reaction carried out by TDO has been shown to be at least partially rate-limited by the initial deprotonation of the L-Trp, on the basis of the H/D kinetic isotope effect of ~4.[34] The importance of the NH group of the indole ring in the oxygen chemistry carried out by the dioxygenases has been demonstrated by Cady and Sono decades ago.[56] It was shown that the methylation of the NH group or its substitution with a sulfur or oxygen atom abolished the enzymatic activity. In addition, the inclusion of an electron-donating group in the indole ring of L-Trp facilitates the oxygen chemistry, whereas the addition of an electron-withdrawing group to the ring retards the reaction.[1] Furthermore, Makino et al. showed that the attachment of an electron withdrawing group to the porphyrin macrocycle slows down the oxygen reaction of L-Trp.[57] These data fully support the ionic mechanism described above and demonstrate that the deprotonation of L-Trp is involved in the rate-limiting step of the reaction.

On the basis of comparative studies, Batabyal and Yeh proposed that the active base deprotonating the L-Trp is the H76 in hTDO, whereas that in hIDO is the heme-bound dioxygen (see the bottom cartoon in Scheme 1).[24] The results reported here underscore the critical role of this evolutionarily conserved H76 in hTDO as the base catalyst, as well as a

structural conduit for the positioning of the indole ring of the L-Trp in a regioorientation favoring the electrophilic addition reaction of the heme-bound O_2 to the C_2=C_3 bond of the L-Trp in the active ternary complex (Figure S4 in the Supporting Information).

In contrast to what is observed in hTDO, Thackray et al. showed that the mutation of the H55 to serine or alanine in xcTDO causes its k_{cat} toward L-Trp to decrease by a factor of 7, regardless of the nature of the substituent for the H55, whereas the K_M remains almost unchanged, as listed in Table 2.[44] The distinct response of xcTDO and hTDO to the mutation of the H55 and H76 residues, respectively, like their differences in the activities toward D- and L-Trp,[18,21,24] reflects the fundamental differences between the two enzymes, despite the fact that they share ~34% sequence homology and that most of the critical distal residues are conserved.[21] One possible structural difference in the active site that may account for the differential activities of xcTDO and hTDO is the replacement of the Y113 in xcTDO with Phe in hTDO, as the Y113 in xcTDO plays a critical role in anchoring the substrate in its active site by forming an H-bond with the carboxylate group of the L-Trp; the loss of the hydroxide group on the Y113 residue may significantly disturb the substrate–protein interactions in hTDO. The understanding of the differences between human and bacterial TDO would certainly improve our knowledge regarding the evolution of the structure and function of TDO family of enzymes.

On the basis of the activity studies of the wild type and H55S and H55A mutants of xcTDO, Forouhar et al.[21] and Thackray et al.[44] proposed that the H55 does not act as an active site base during the oxygen reaction, based on two observations: (1) the activity is insensitive to pH from 6–8.3, and (2) the mutations in the H55 do not completely abolish the activity of the enzyme. In our view, this evidence is not strong enough to exclude the base-catalyst role of H55, considering the fact that: (1) it has been demonstrated in rat liver TDO that the rate-limiting step of the reaction is altered as the pH is raised to 8, on the basis of kinetic isotope effect measurements,[34] and (2) the presence of an alternative base in the active site of the mutants, such as a water molecule as we proposed here, may account for the residual activities of the mutants.

Conclusions

Resonance Raman data indicate that the substrate L-Trp is positioned in the active site by the polar interactions between the ammonium and carboxyl groups of the L-Trp and the protein matrix, as well as the hydrophobic interactions between the aromatic indole ring and its surroundings, including the imidazole ring of the H76. The activity studies show that the mutation of the H76 residue to serine and alanine causes 70 and 10-fold decrease in the k_{cat} value and the 6 and 3-fold increase in the K_M value, respectively. Taken together the data support the scenario that, during the dioxygenase reaction, the H76 residue functions as a base catalyst to deprotonate the indole NH group of the L-Trp, the initial step of reaction. In addition, it acts as a structural conduit to position the indole ring of the L-Trp in a proper regioorientation favoring the electrophilic addition reaction of the heme-bound O_2 to the C_2=C_3 bond of the L-Trp. We hypothesize that the residual activities of the mutants are due to the replacement of the active site base catalyst, H76, with a weaker base, possibly an active site water. Optical absorption data show that the substrate-free hTDO binds O_2 to

form a metastable O_2-complex, contrary to the general belief that TDO does not bind O_2 without the substrate. The perturbation in the electronic properties of the O_2-complex of hTDO introduced by L-Trp binding and the sensitivity of the electronic properties of the active ternary complex, L-Trp-O_2-hTDO, to the mutation in the H76 residue further support the role of H76 in regulating the tight substrate–protein interactions in hTDO. In summary, the data reported here demonstrate that the H76 residue plays a critical role in modulating the oxygen chemistry of hTDO by controlling substrate binding and the deprotonation of the indole NH group of the L-Trp. These data establish an important basis for our current understanding of the oxygen chemistry carried out by heme-containing dioxygenases.

Supplementary Material

Refer to Web version on PubMed Central for supplementary material.

Acknowledgments

We thank Drs. Denis L. Rousseau, Changyuan Lu, Tsuyoshi Egawa, and Mr. Ariel Lewis for valuable discussions, Mr. Jaime Anguiano for the mutagenesis work, and Mr. Anirban Ray for the kind help in western blot analysis of the purified hTDO protein.

References

1. Sono M, Roach MP, Coulter ED, Dawson JH. Chem Rev. 1996; 96(7):2841–2888. [PubMed: 11848843]
2. Hayaishi O. J Biochem (Tokyo). 1976; 79:13–21.
3. Feigelson, O.; Brady, FO. Molecular Mechanism of Oxygen Activation. Hayaishi, O., editor. Academic Press; New York: 1974. p. 87-133.
4. Hayaishi O, Takikawa O, Yoshida R. Prog Inorg Chem. 1990; 38:75.
5. Schutz G, Feigelson P. J Biol Chem. 1972; 247:5327–5332. [PubMed: 4626718]
6. Greengard O, Feigelson P. J Biol Chem. 1961; 236:158–161. [PubMed: 13708324]
7. Knox WE, Mehler AH. J Biol Chem. 1950; 187:419. [PubMed: 14794727]
8. Takikawa O. Biochem Biophys Res Commun. 2005; 338(1):12–19. [PubMed: 16176799]
9. Yamamoto S, Hayaishi O. J Biol Chem. 1967; 242(22):5260–5266. [PubMed: 6065097]
10. Muller AJ, Prendergast GC. Curr Cancer Drug Targets. 2007; 7(1):31–40. [PubMed: 17305476]
11. Ishiguro I, Naito J, Nagamura Y. FEBS Lett. 1993; 329:178–182. [PubMed: 8354392]
12. Miller CL, Llenos IC, Dulay JR, Barillo MM, Yolken RH, Weis S. Neurobiol Dis. 2004; 15:618–629. [PubMed: 15056470]
13. Munn DH, Mellor AL. J Clin Invest. 2007; 117(5):1147–1154. [PubMed: 17476344]
14. Schutz G, Killewich L, Chen G, Feigelson P. Proc Natl Acad Sci U S A. 1975; 72(3):1017–1020. [PubMed: 1055360]
15. Schimke RT, Sweeney EW, Berlin CM. J Biol Chem. 1965; 240:322–331. [PubMed: 14253432]
16. Shimizu T, Nomiyama S, Hirata F, Hayaishi O. J Biol Chem. 1978; 253(13):4700–4706. [PubMed: 26687]
17. Hirata F, Hayaishi O. Biochem Biophys Res Commun. 1972; 47(5):1112–1119. [PubMed: 4537396]
18. Ishimura Y, Nozaki M, Hayaishi O. J Biol Chem. 1970; 245(14):3593–3602. [PubMed: 5470825]
19. Taniguchi T, Sono M, Hirata F, Hayaishi O, Tamura M, Hayashi K, Iizuka T, Ishimura Y. J Biol Chem. 1979; 254(9):3288–3294. [PubMed: 218967]
20. Sugimoto H, Oda S, Otsuki T, Hino T, Yoshida T, Shiro Y. Proc Natl Acad Sci USA. 2006; 103(8):2611–2616. [PubMed: 16477023]

21. Forouhar F, et al. Proc Natl Acad Sci USA. 2007; 104(2):473–478. [PubMed: 17197414]
22. Zhang Y, Kang SA, Mukherjee T, Bale S, Crane BR, Begley TP, Ealick SE. Biochemistry. 2007; 46(1):145–155. [PubMed: 17198384]
23. Dick RMB, Reid MJ, Correia MA. Arch Biochem Biophys. 2001; 392(1):71–78. [PubMed: 11469796]
24. Batabyal D, Yeh SR. J Am Chem Soc. 2007; 129(50):15690–15701. [PubMed: 18027945]
25. Terentis AC, Thomas SR, Takikawa O, Littlejohn TK, Truscott RJ, Armstrong RS, Yeh SR, Stocker R. J Biol Chem. 2002; 277(18):15788–15794. [PubMed: 11867636]
26. Gaspari P, Banerjee T, Malachowski WP, Muller AJ, Prendergast GC, DuHadaway J, Bennett S, Donovan AM. J Med Chem. 2006; 49(2):684–692. [PubMed: 16420054]
27. Pereira A, Vottero E, Roberge M, Mauk AG, Andersen RJ. J Nat Prod. 2006; 69(10):1496–1499. [PubMed: 17067170]
28. Botting NP. Chem Soc Rev. 1995; 24:401–412.
29. Basran J, Rafice SA, Chauhan N, Efimov I, Cheesman MR, Ghamsari L, Raven EL. Biochemistry. 2008; 47:4752–4760. [PubMed: 18370401]
30. Manandhar SPSH, Nagano S, Egawa T, Ishimura Y. Int Congr Ser. 2002; 1233:161–169.
31. Feigelson P, Greengard O. J Biol Chem. 1962; 237:1908–1913. [PubMed: 13892027]
32. Li JS, Han Q, Fang J, Rizzi M, James AA, Li J. Arch Insect Biochem Physiol. 2006; 64:74–87. [PubMed: 17212352]
33. Watanabe Y, Fujiwara M, Yoshida R, Hayaishi O. Biochem J. 1980; 189(3):393–405. [PubMed: 6783035]
34. Leeds JM, Brown PJ, McGeehan GM, Brown FK, Wiseman JS. J Biol Chem. 1993; 268(24): 17781–17786. [PubMed: 8349662]
35. Ren S, Liu H, Licad E, Correia MA. Arch Biochem Biophys. 1996; 333(1):96–102. [PubMed: 8806758]
36. Egawa T, Yeh SR. J Inorg Biochem. 2005; 99(1):72–96. [PubMed: 15598493]
37. Spiro, TG.; Li, XY. Biological applications of Raman Spectroscopy. John Wiley and Sons; New York: 1988.
38. Wang, J.; Caughey, WS.; Rousseau, DL. Methods in Nitric Oxide research. John Wiley & Sons; New York: 1996. Resonance Raman Scattering; p. 427-454.
39. Kitagawa T, Ozaki Y. Struct Bonding (Berlin). 1987; 64:71–114.
40. Yu, NT.; Kerr, EA. Biological Applications of Raman Spectroscopy. John Wiley and Sons; New York: 1988. Resonance Raman Spectra of heme and metallo proteins; p. 39-95.
41. Makino R, Sakaguchi T, Iizuka T, Ishimura Y. J Biol Chem. 1980; 255:11883–11891. [PubMed: 6254984]
42. Uchida K, Shimizu T, Makino R, Sakaguchi K, Iizuka T, Ishimura Y, Nozawa T, Hatano M. J Biol Chem. 1983; 258(4):2519–2525. [PubMed: 6600455]
43. Hu S, Smith KM, Spiro TG. J Am Chem Soc. 1996; 118:12368–12646.
44. Thackray SJ, Bruckmann C, Anderson JL, Campbell LP, Xiao R, Zhao L, Mowat CG, Forouhar F, Tong L, Chapman SK. Biochemistry. 2008; 47(40):10677–10684. [PubMed: 18783250]
45. Mendel S, Arndt A, Bugg TD. Biochemistry. 2004; 43(42):13390–13396. [PubMed: 15491145]
46. Sligar SG, Makris TM, Denisov IG. Biochem Biophys Res Commun. 2005; 338(1):346–354. [PubMed: 16139790]
47. Li D, Kabir M, Stuehr DJ, Rousseau DL, Yeh SR. J Am Chem Soc. 2007; 129(21):6943–6951. [PubMed: 17488012]
48. Unno M, Matsui T, Chu GC, Couture M, Yoshida T, Rousseau DL, Olson JS, Ikeda-Saito M. J Biol Chem. 2004; 279(20):21055–21061. [PubMed: 14966119]
49. Martin NI, Woodward JJ, Winter MB, Beeson WT, Marletta MA. J Am Chem Soc. 2007; 129(41): 12563–12570. [PubMed: 17892291]
50. Ishimura Y, Nozaki M, Hayaishi O. J Biol Chem. 1967; 242(10):2574–2576. [PubMed: 6026250]
51. Li T, Quillin ML, Phillips GN Jr, Olson JS. Biochemistry. 1994; 33(6):1433–1446. [PubMed: 8312263]

52. Spiro TG, Wasbotten IH. J Inorg Biochem. 2005; 99(1):34–44. [PubMed: 15598489]
53. Uchida TIH, Ishimori K, Morishima I, Nakajima H, Aono S, Mizutani Y, Kitagawa T. Biochemistry. 2000; 39:12747–12752. [PubMed: 11041838]
54. Jeyarajah S, Proniewicz LM, Bronder H, Kincaid JR. J Biol Chem. 1994; 269(49):31047–31050. [PubMed: 7983043]
55. Hamilton GA. Adv Enzymol Relat Areas Mol Biol. 1969; 32:55–96. [PubMed: 4978050]
56. Cady SG, Sono M. Arch Biochem Biophys. 1991; 291:326–331. [PubMed: 1952947]
57. Makino, R.; Iizuka, T.; Sakaguchi, K.; Ishimura, Y. Oxygenases and oxygen metabolism. Academic Press; New York: 1980. p. 467-477.
58. Hagarman A, Wallace CJ, Laberge MM, Schweitzer-Stenner R. Out-of-plane deformations of the heme group in different ferrocytochrome c proteins probed by resonance Raman spectroscopy. J Raman Spectrosc. 2008; 39:1848–1858.

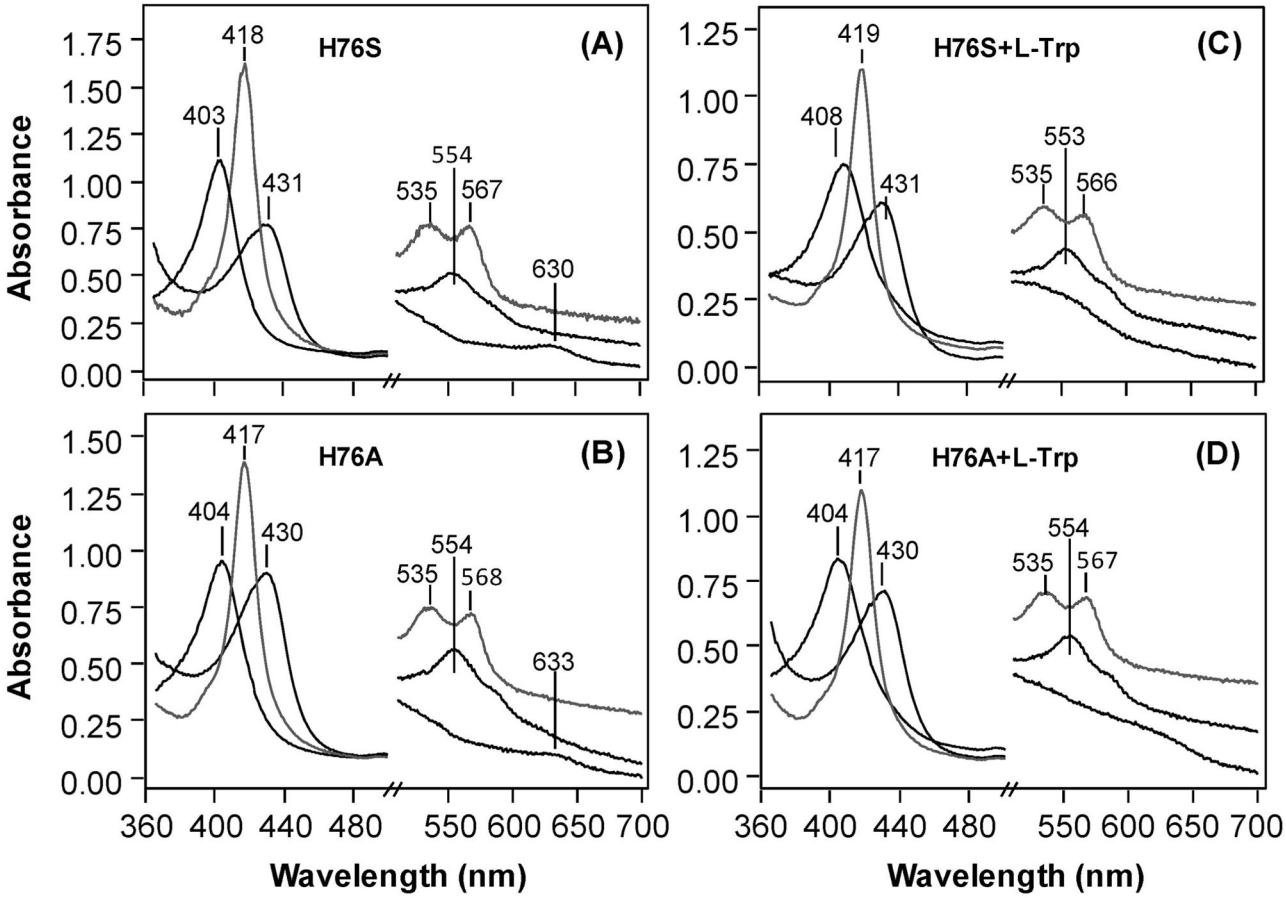

Figure 1.

Optical absorption spectra of the ferric, ferrous, and CO-derivatives of the H76S and H76A mutants of hTDO in the absence (A and B) and presence (C and D) of L-Trp. The visible bands are expanded by a factor of 4 and are staggered for clarity. The protein solutions were buffered at pH 7 with 100 mM phosphate. The concentration of L-Trp used for C and D was 20 mM.

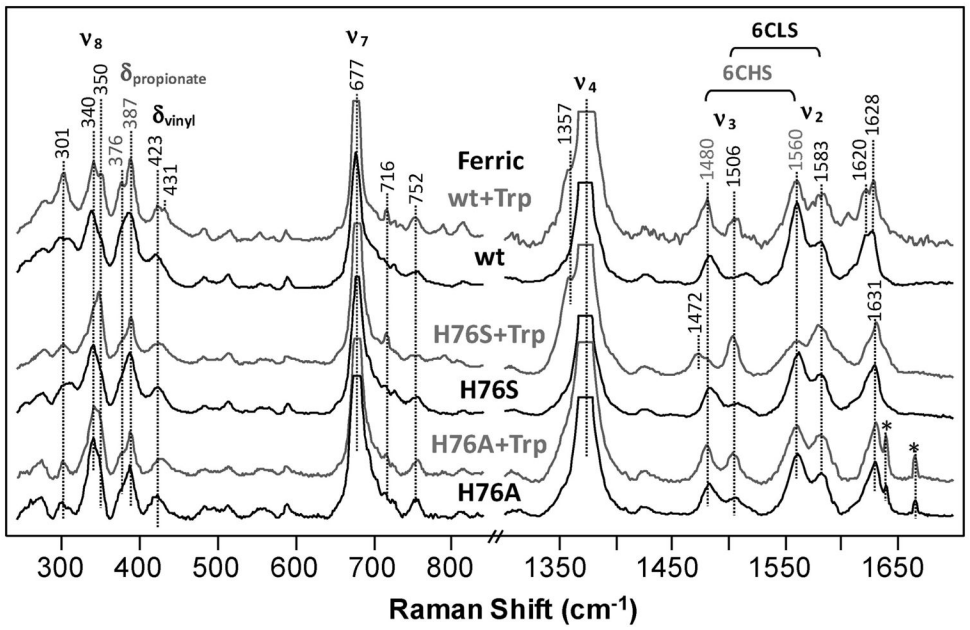

Figure 2.

Resonance Raman spectra of the ferric derivative of the H76S and H76A mutants of hTDO, with respect to the wild type enzyme, in the presence and absence of L-Trp. The small shoulder at 1357 cm^{-1} in the L-Trp bound wild type and H76S mutant is a result of a small amount of photoinduced reduction of the ferric heme. The protein concentrations are ~25–40 μM. The protein solutions were buffered at pH 7 with 100 mM phosphate. The concentration of L-Trp was 20 mM. The excitation wavelength for the Raman measurements was 413.1 nm and the laser power was ~5 mW. The sharp peaks labeled with asterisks are the plasma lines from the laser.

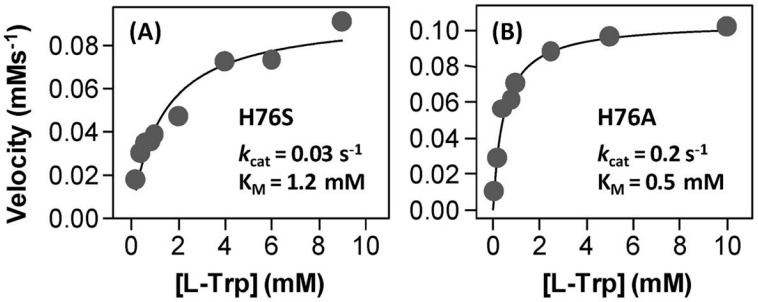

Figure 3.

Activity assay of the H76S (A) and H76A (B) mutants of hTDO. The activities were measured with 3.5 μM H76S (A) and 0.5 μM H76A (B). The solid lines show the Michaelis–Menten curves best fit the data. The k_{cat} and K_M obtained from the fits are as indicated.

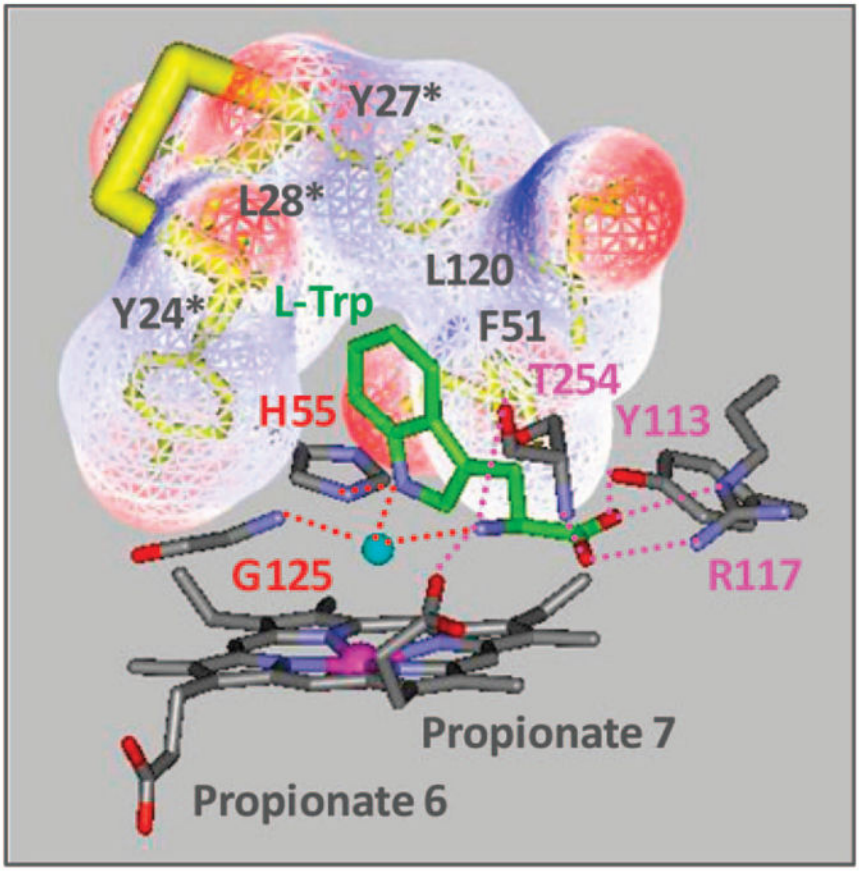

Figure 4.

Distal pocket structure of the L-Trp-bound xcTDO. The PDB code is 2NW8. The cyan sphere, which occupies part of the ligand binding site, is a water molecule. The residues that make up the hydrophobic pocket housing the aromatic indole ring of the substrate are labeled in black. The residues labeled with asterisks, which are attached to the peptide region labeled in yellow, are from another subunit of the tetrameric enzyme. The H-bonding interactions that stabilize the L-Trp are indicated by the dotted lines. The residues labeled in magenta are important in forming H-bonds with the ammonium and carboxylate group of the L-Trp. The H55 and G125 correspond to the H76 and G152 in hTDO, respectively.

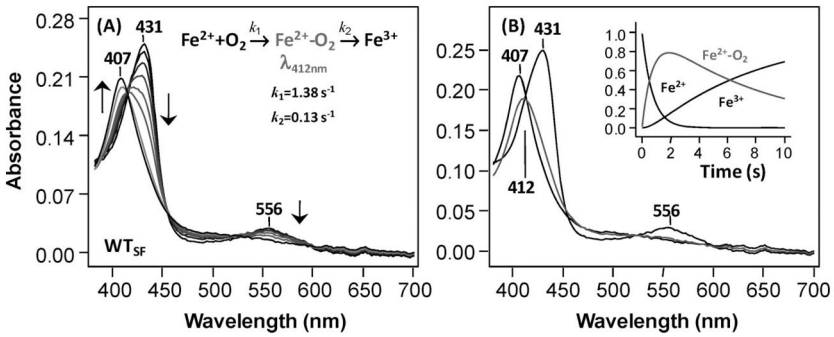

Figure 5.

Reaction of the wild type ferrous deoxy hTDO with O_2. The spectra shown in (A) were obtained as a function of time following the mixing of the ferrous deoxy enzyme with air-saturated buffer. The standard spectra of the ferrous deoxy species, O_2-complex and the ferric species obtained from global analysis of the data shown in (A) based on a three-state sequential model are shown in (B). The time evolutions of the three standard species are shown in the inset. The samples were prepared in 100 mM phosphate (pH 7) as described in the text.

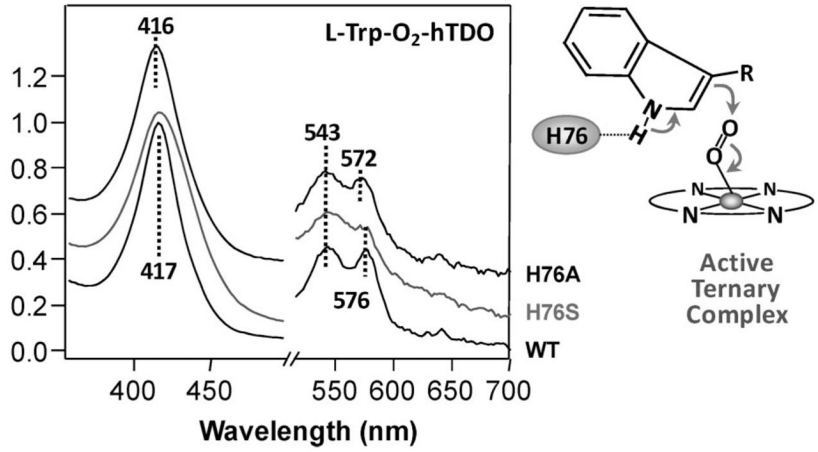

Figure 6.

Optical absorption spectra of the ternary complex (LTrp-O_2-hTDO) of the wild type and the H76S and H76A mutants of hTDO. The visible bands are expanded by a factor of 4 and are staggered for clarity. The samples were prepared in 100 mM phosphate (pH 7) as described in the text. The concentration of L-Trp was 10 mM. Right panel shows the hypothesized structure of the active ternary complex of hTDO.

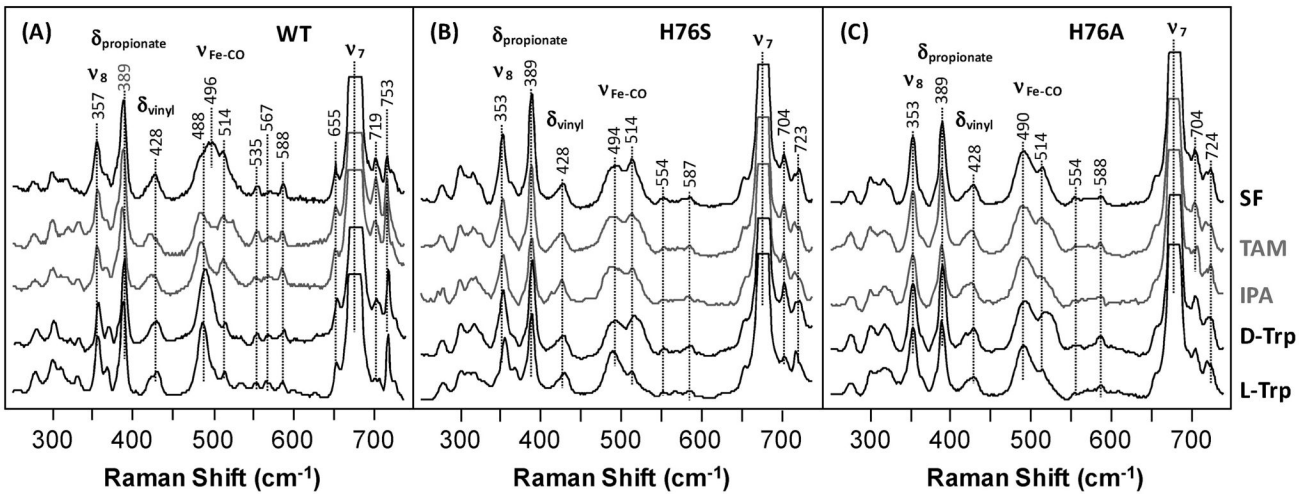

Figure 7.

Resonance Raman spectra of the CO-derivative of the wild type and the H76S and H76A mutants of hTDO in the presence and absence of Trp and Trp analogs. The concentration of Trp or Trp analog is 26 mM. “SF” stands for substrate-free. The excitation wavelength for the resonance Raman measurements was 413.1 nm and laser power was about ~1–2 mW. The structures of TAM, IPA and Trp are shown in Scheme 2. The scheme on the left shows the hypothesized structures of the various conformers of the wild type protein, with Trp or Trp analog bound to them, as discussed in the text.

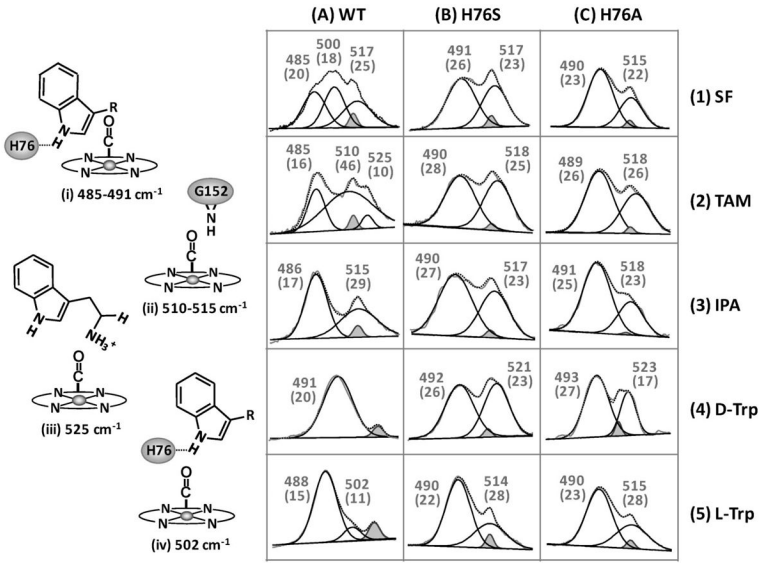

Figure 8.

$\nu_{Fe\text{-}CO}$ modes of the wild type and H76S and H76A mutants of hTDO in the presence or absence of Trp and Trp analogs. The data were taken from Figure 7. “SF” stands for substrate-free. Each $\nu_{Fe\text{-}CO}$ mode was deconvoluted into a minimum set of Gaussian peaks, as shown under each mode. Each peak maximum is indicated; the line width is shown in the parenthesis. It is important to note that the physical line widths of the peaks appearing in the figure are comparable within each panel, but not comparable between the panels, as the *x* axes are not the same for the panels. The small Gaussian peak at 514 cm^{-1} colored in gray, which is present in every spectrum, is an intrinsic heme mode; it is not labeled for clarity. The similarity between the raw data (solid curve) and the best-fitted spectra (dotted curve) demonstrates the reliability of the deconvolution method. (Left) Scheme illustrating four possible conformers (i–iv) of the Trp or Trp analog-bound wild type hTDO, along with their associated $\nu_{Fe\text{-}CO}$ frequencies.

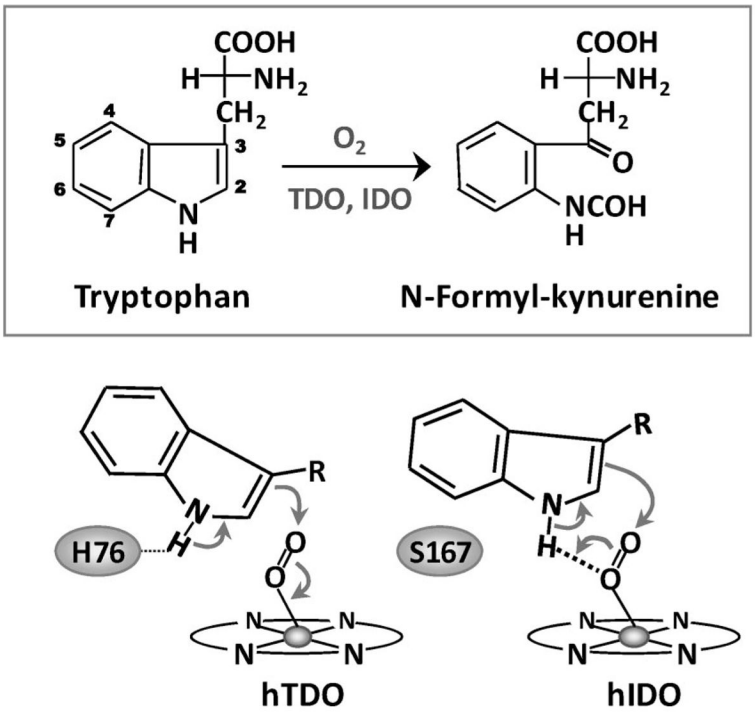

Scheme 1.

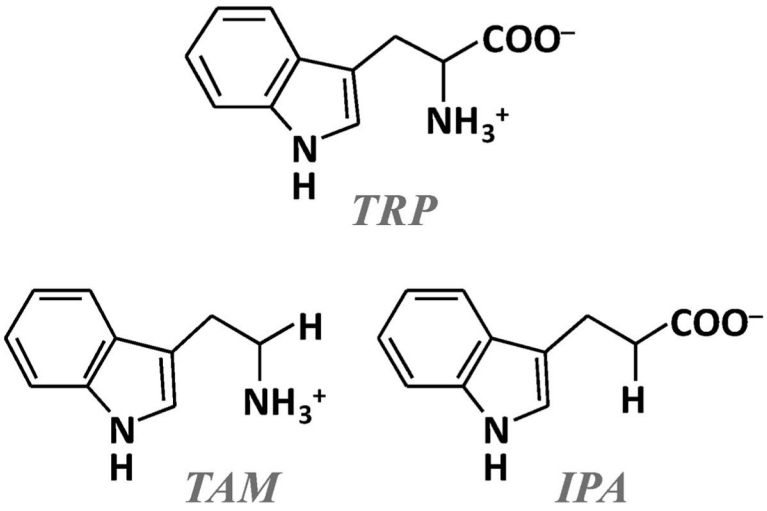

Scheme 2.

Table 1

Iron-Ligand Stretching Frequencies (cm^{-1}) and Soret and Visible Absorption Maxima (nm) of the Wild Type and the H76S and H76A Mutants of hTDO

		$\nu_{Fe\text{-}His}$ [a]	$\nu_{Fe\text{-}CO}$ [a]	λ_{ferric} [b]	$\lambda_{ferrous}$ [b]	λ_{CO} [b]
WT	SF[c]	229	485, 500, 517	406, 633	432, 556	420, 538/568
	L-Trp	229	488,502	407	433, 555	421, 537/567
	D-Trp	nd	491	406	432, 558	421, 569
H76A	SF[c]	228	490, 515	404, 633	430, 554	417, 535/568
	L-Trp	228	490, 515	404	430, 554	417, 534/567
	D-Trp	nd	493, 523	404	430, 554	417, 534/568
H76S	SF[c]	228	490, 517	403, 630	430, 554	417, 535/568
	L-Trp	228	490, 514	408	431, 553	419, 535/566
	D-Trp	nd	492, 521	404	431, 554	417, 536/568

[a] Data are taken from Figure 8.

[b] Values are absorption maxima of the Soret and visible bands.

[c] "SF" stands for substrate-free.

Table 2

Kinetic Constants Defining the Activities of the Wild Type and Mutants of hTDO and xcTDO towards L-Trp

		k_{cat} (s^{-1})	K_M (mM)	k_{cat}/K_M	reference
hTDO	Wild type	2.1	0.19	11.05	[24]
	H76A	0.2	0.5	0.4	This work
	H76S	0.03	1.2	0.025	This work
xcTDO	Wild type	19.5	0.114	171	[21]
	H55A	2.86	0.133	21.5	[21]
	H55S	2.6	0.197	13.1	[44]